



# Pinning platinum and Pt-oxide nanoparticles on graphite

Jianzhi Gao, Quanmin Guo\*

School of Physics and Astronomy, University of Birmingham, Edgbaston, Birmingham, B15 2TT, United Kingdom

## ARTICLE INFO

### Article history:

Received 4 January 2012

Accepted 7 February 2012

Available online 15 February 2012

### Keywords:

Pt clusters

Platinum

Graphite

Oxidation

Catalysis

Scanning tunnelling microscopy (STM)

Surface defects

Adsorption

## ABSTRACT

Nanoparticles of platinum oxide are deposited onto a highly oriented pyrolytic graphite (HOPG) substrate. The platinum oxide particles are formed by flowing oxygen gas through a hot (1425 K) platinum capillary tube in vacuum. By controlling the temperature and the gas flow, a condition can be reached so that Pt atoms are evaporated from the inner walls of the tube and subsequently oxidised by oxygen either before or after landing on HOPG. Atomic oxygen, produced inside the tube through thermal cracking of  $O_2$ , is co-deposited onto HOPG. Atomic oxygen form strong bonds with carbon atoms on the HOPG surface and hence a significant number of pinning sites are created for the incoming platinum and platinum oxide particles.

© 2012 Elsevier B.V. All rights reserved.

## 1. Introduction

Small metal clusters play an important role in heterogeneous catalysis [1,2]. In order to understand the fundamental mechanism of reactivity and selectivity of supported metal catalysts, a large number of model systems, mostly consisting of small metal particles on metal oxide supports, have been designed and studied [3–7]. From a very early stage it was recognised that the metal-support interaction strongly influences the performance of the metal particles [8,9] and the phenomenon of strong-metal-support-interaction (SMSI) has been investigated extensively ever since it was discovered [10–13]. In order to keep the metal particles catalytically active, the metal support interaction should be optimised. Too strong an interaction causes encapsulation of the metal by the metal oxide support, and too weak an interaction is unable to keep the metal particles in a well-dispersed state leading to aggregation and loss of effective surface area. Here we examine the situation where the metal-support interaction is weak, and hence seek a method to pin metal particles and prevent them from sintering. We have chosen graphite, highly oriented pyrolytic graphite (HOPG), as the substrate for its known inertness towards many metals. There is a large body of data in literature regarding the interaction of metal atoms/clusters with HOPG [14–26]. Recently, stimulated by the discovery of graphene, there is a rapid increase in the number of publications of metal deposition on

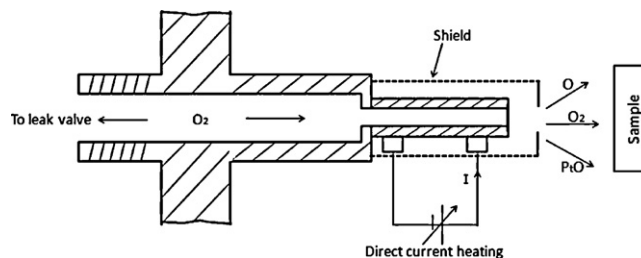
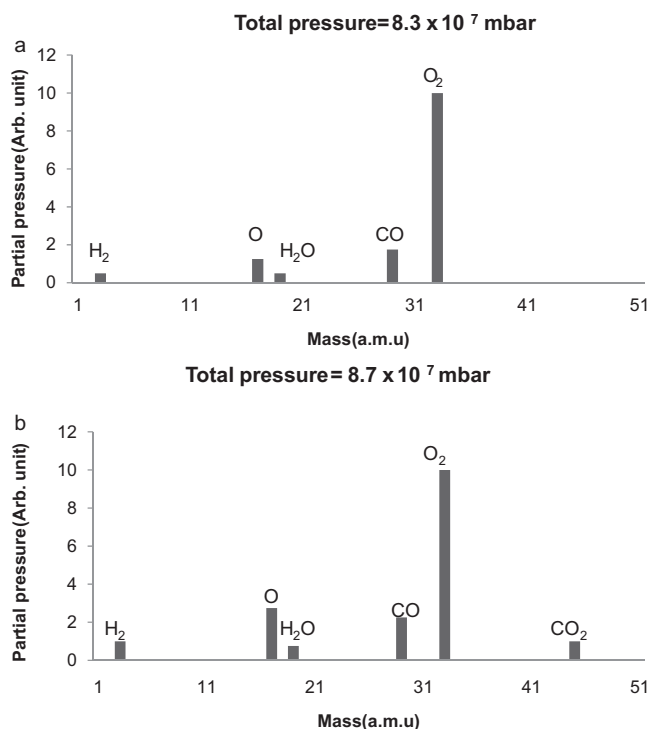


Fig. 1. Schematic diagram of the oxygen thermal cracking source.

graphene [27–29]. Both individual atoms and clusters of metals are very mobile on HOPG due to low diffusion barriers [14,15,17]. As a result, deposited metal atoms or clusters tend to aggregate along the step edges. In order to fix metal clusters on HOPG, pre-fabricated surface atomic defects produced by  $Ar^+$  ion sputtering for example [22] are used. An alternative method is to allow the metal clusters to impinge onto HOPG with high kinetic energies [19,24,25]. Defects generated by  $Ar^+$  ion sputtering or energetic clusters are usually not confined just to the top layer of carbon and are inevitably linked to physical damage to the graphite surface. Here we report a procedure for fixing Pt oxide particles without causing gross physical damage to the graphite substrate. By using a heated Pt capillary tube, we are able to co-deposit Pt oxide nanoparticles and atomic oxygen onto HOPG simultaneously. The adsorbed atomic oxygen is able to pin the Pt metal oxide particles. The fixing of Pt and PtO particles on graphite is an important process because

\* Corresponding author. Tel.: +44 1214144657; fax: +44 1214147327.  
E-mail address: [Q.Guo@bham.ac.uk](mailto:Q.Guo@bham.ac.uk) (Q. Guo).



**Fig. 2.** Mass spectra of gases inside the vacuum chamber, recorded with a quadrupole mass spectrometer as molecular oxygen passes through the Pt tube kept at (a) room temperature and (b) at 1423 K.

graphite-supported Pt catalysts are used for liquid-phase oxidation of organic molecules [30,31] in fuel cell applications.

## 2. Experimental

Experiments are performed in an ultra-high vacuum (UHV) system equipped for variable temperature scanning tunnelling microscopy (Omicron VT-STM) with a base pressure of  $2 \times 10^{-10}$  mbar. Electrochemically polished tungsten tips are used and images are acquired using bias voltages from 0.005 V to

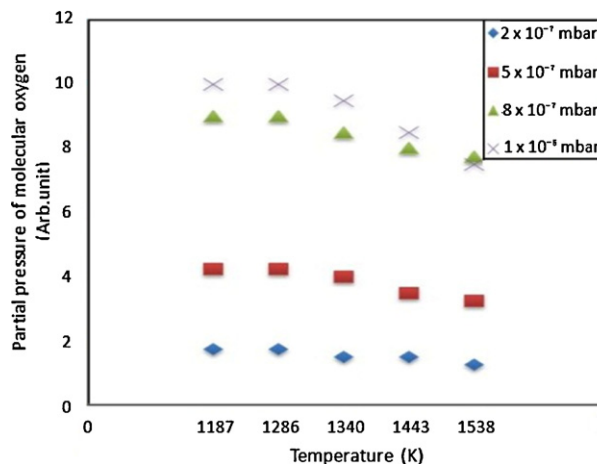


**Fig. 3.** Partial pressure of  $O_2$  as a function of capillary tube temperature.

1.0V, with tunnel current from 0.03 nA to 1 nA. Highly oriented pyrolytic graphite sample was cleaved in air and further cleaned in UHV by degassing at 1000 K for 30 min. A homemade thermal cracking source is used to deliver atomic oxygen and Pt/PtO onto the HOPG sample. Fig. 1 shows a schematic diagram of the thermal cracking source. It consists of a Pt capillary tube with 0.4 mm inner diameter and 0.7 mm outer diameter. The tube can be heated to 1600 K by passing a direct current with or without the flow of oxygen. A cylindrical shield with an aperture is used to cover the Pt tube so that only material coming out from the inner tube can reach the sample.

## 3. Results and discussion

First of all, we would like to describe the properties of the cracking source. We use a quadrupole mass spectrometer to monitor the gas composition as a function of the capillary tube temperature and gas flow rate. Fig. 2a shows the gas composition when oxygen is passed through the Pt tube without heating. The total pressure inside the vacuum chamber during the measurement is  $8.3 \times 10^{-7}$  mbar, and this is mainly due to molecular oxygen.  $O_2$

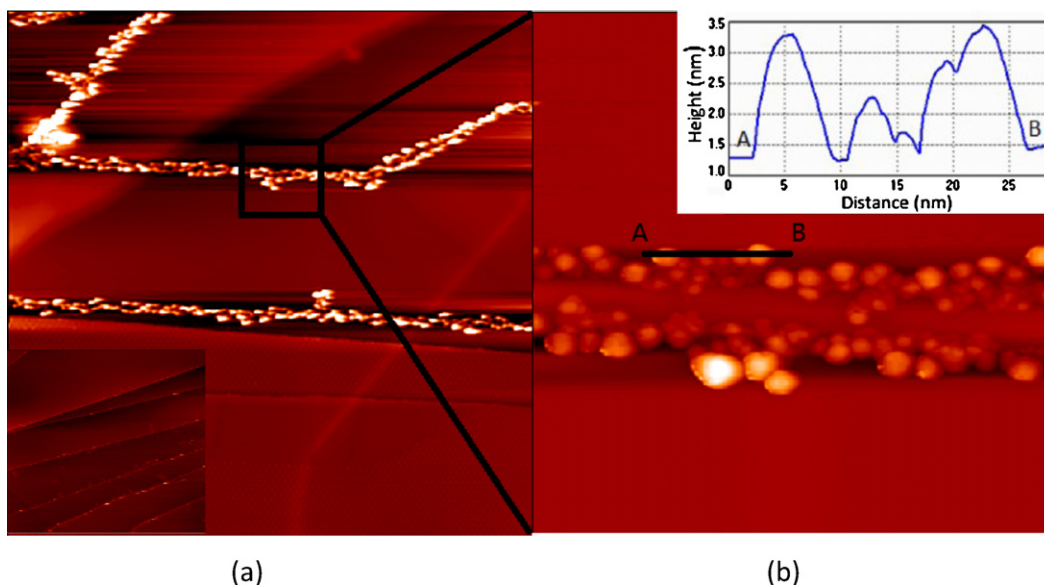


**Fig. 4.** (a) STM image, 700 nm  $\times$  700 nm, of HOPG after deposition of Pt. Image acquired using  $-0.5$  V sample bias and 0.3 nA tunnel current. Inset at the lower left corner shows the HOPG surface before the deposition of Pt. (b) Zoomed-in view, 100 nm  $\times$  100 nm, of the area inside the black square in (a). Inset shows the height profile along line A–B.

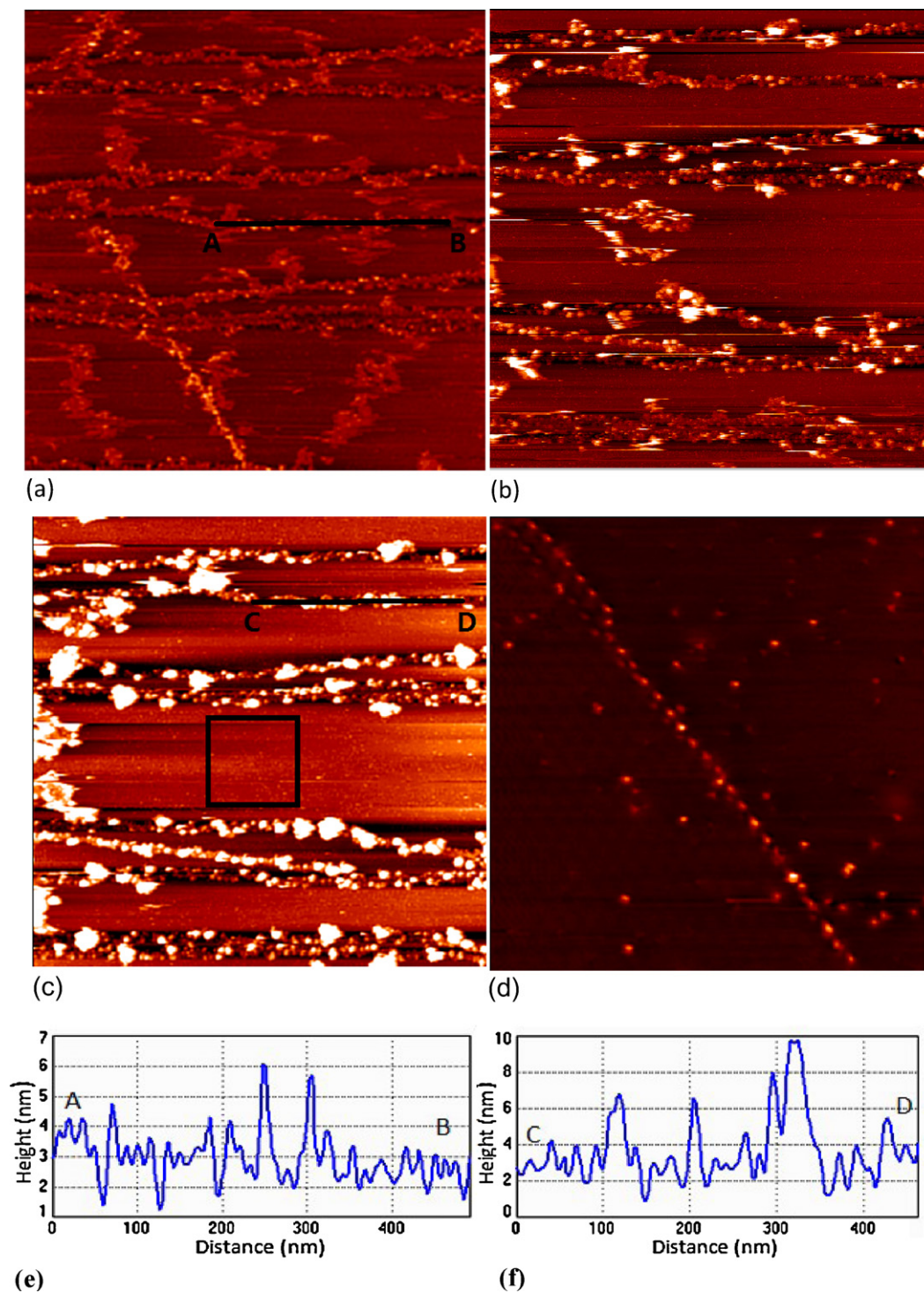


**Fig. 5.** (a) STM image,  $1000 \text{ nm} \times 1000 \text{ nm}$ , of HOPG after co-deposition of Pt/PtO and atomic oxygen. Image acquired using  $+0.5 \text{ V}$  sample bias and  $0.03 \text{ nA}$  tunnel current. (b) Same as (a) but image acquired after 5 min scanning at room temperature. (c) STM image,  $1000 \text{ nm} \times 1000 \text{ nm}$ , showing the displacement of material by the STM tip from terraces and re-deposition at step edges. (d) Zoomed-in view,  $180 \text{ nm} \times 180 \text{ nm}$ , of the area inside the black square in (c). Image obtained using  $+0.4 \text{ V}$  sample bias and  $0.6 \text{ nA}$  tunnel current. The bright spots on the terraces are due to chemically bonded oxygen atoms. (e) Height profile along line AB in (a). (f) Height profile along line CD in (c).

together with its cracking product, atomic oxygen produced in the ionisation chamber of the mass spectrometer, is observed alongside  $\text{CO}$ ,  $\text{H}_2$ , and  $\text{H}_2\text{O}$ . There is also  $\text{CO}_2$ , but its signal is low and is not visible on the same scale. Fig. 2b shows the measured gas composition when the Pt tube is heated to  $1423 \text{ K}$ . The temperature of the Pt tube is measured using an optical pyrometer. We notice a significant increase in the signals corresponding to atomic oxygen at mass  $16 \text{ amu}$  and  $\text{CO}_2$  at mass  $44 \text{ amu}$ . Although we

expect the production of atomic oxygen via thermal cracking, we do not think the increased O signal is due to the direct interception of O from the Pt tube by the mass spectrometer. This is because the mass spectrometer is not arranged in direct line-of-sight configuration with the Pt tube, hence atomic oxygen from the tube cannot reach the mass spectrometer without bouncing from something else in the vacuum chamber. The increased level of O signal, we believe, comes from an increased fraction of thermally excited

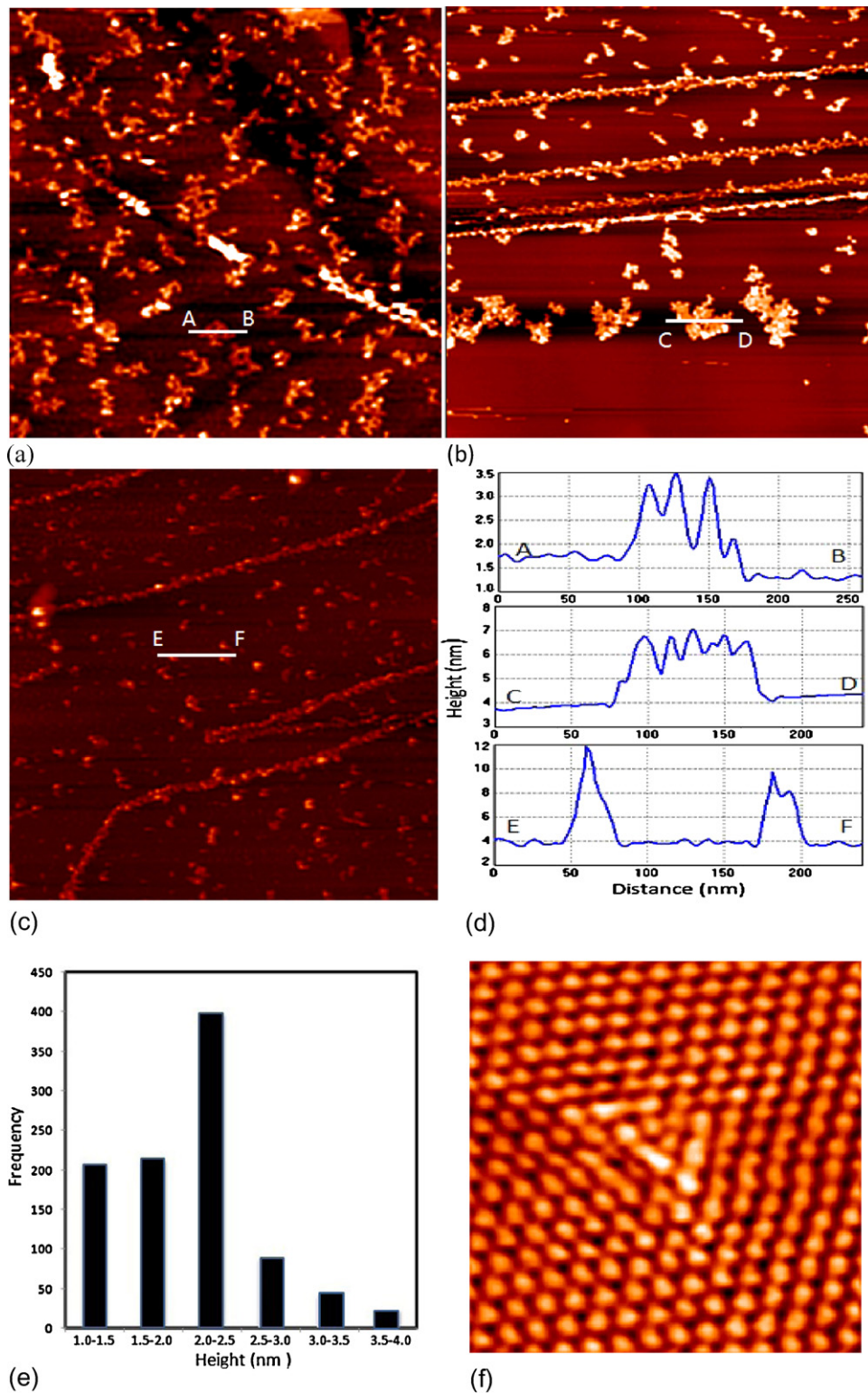


**Fig. 6.** (a) STM image,  $1000 \text{ nm} \times 1000 \text{ nm}$ , of HOPG with deposited PtO following thermal annealing to 473 K in UHV. Image was obtained using  $-0.5 \text{ V}$  sample bias and  $0.03 \text{ nA}$  tunnel current. (b) The same sample after thermal annealing to 773 K. (c) The same sample after thermal annealing to 973 K. (d) Height measurement for line AB, CD, and EF respectively. (e) Height distribute statistics of (a). (f) Atomically resolved STM image obtained using  $-0.2 \text{ V}$  sample bias and  $0.8 \text{ nA}$  tunnel current,  $3 \text{ nm} \times 3 \text{ nm}$ , showing the detailed structure induced by the adsorption of atomic oxygen.

molecular oxygen. The higher concentration of excited molecular oxygen alters the cracking pattern of  $\text{O}_2$  inside the ionisation chamber of the mass spectrometer in favour of the production of atomic ions. Some excited molecules on contact with the chamber walls will dissociate, resulting in the formation of atomic oxygen.

Subsequent reaction between atomic oxygen and carbon containing species produces  $\text{CO}_2$  as observed with the mass spectrometer.

Accompanied by the increase in atomic oxygen signal, there is a drop in molecular oxygen signal. This drop occurs at  $\sim 1300 \text{ K}$  and seems to be independent of the oxygen flow rate. Fig. 3 shows

how  $O_2$  signal decreases with temperature for a range of oxygen flow rates. The equilibrium partial pressure of  $O_2$  inside the vacuum chamber is used as a measure of the flow rate.

The drop of  $O_2$  partial pressure can be contributed by more than one factor. The most obvious one is the consumption of  $O_2$  by thermal cracking into atomic oxygen inside the Pt tube. Atomic oxygen then reacts on chamber walls giving out CO and  $CO_2$ . A related factor is the formation of thermally excited molecular oxygen. As mentioned earlier, some of the excited oxygen molecules can dissociate into atomic oxygen after they leave the tube. The third factor is the evaporation of Pt and subsequent reaction of the evaporated Pt atoms with molecular oxygen. All the above three processes consume molecular oxygen. Judging from the characteristics of the deposited material on HOPG as will be shown in the following, Pt evaporation has indeed occurred. At the present time, it is not clear which of the three processes contributes most to the removal of molecular oxygen.

Fig. 4 shows STM images of the HOPG sample with Pt deposited in the absence of oxygen. This experiment was conducted in UHV without any oxygen flowing through the Pt tube. The temperature of the Pt tube was raised to 1423 K and the HOPG sample was then turned to face the opening end of the tube for 3 min. The HOPG sample was held at 723 K during the whole process. STM imaging was performed after cooling the sample down to room temperature. The STM image in Fig. 4a shows the aggregation of Pt particles along the step edges and grain boundaries. Inset in Fig. 4a shows the morphology of the HOPG surface before Pt deposition. Fig. 4b shows a zoomed-in image from the area marked by the black square in Fig. 4a. Inset in Fig. 4b shows a height profiles along the line AB. According to this height profile, the Pt particles on average are  $\sim 1.7$  nm in height. The average lateral dimension of these particles is  $\sim 5$  nm without correcting for tip convolution. By counting the number of particles and using the average volume of the particle based on the height profile data, we estimated that the amount of Pt deposited on HOPG is equivalent to 0.1 ML and hence a deposition flux  $5 \times 10^{12}$  atoms  $cm^{-2} s^{-1}$ . The formation of three-dimensional nanometer-sized metal particles at HOPG step edges is a well-known phenomenon [32–34]. The absence of particles on the flat terraces is a result of very weak metal-substrate interaction, and only impinging particles with excessive kinetic energy can get pinned on the terrace upon landing [24].

We then repeated the above experiment on a freshly cleaved HOPG sample, but this time with oxygen flowing through the tube and sample kept at room temperature. The flow rate was adjusted to give an equilibrium partial pressure of oxygen  $5 \times 10^{-7}$  mbar in the UHV chamber. The temperature of the Pt tube was 1423 K and the sample was exposed for 3 min. Fig. 5a shows the morphology of the surface after deposition. The material deposited on HOPG in this case is Pt oxide. Even if there are Pt atoms coming out of the tube, they must have been oxidised once they land on the HOPG surface due to the presence of the background oxygen atmosphere. If we assume that the flux of Pt atoms stays the same,  $5 \times 10^{12}$  atoms  $cm^{-2} s^{-1}$ , there are more than two orders of magnitude of excess molecular oxygen available to oxidise the Pt. Some Pt oxide is formed inside the tube while the rest is formed on the surface of HOPG. The deposited PtO seems to be weakly attached to the substrate and tip-induced material movement is clearly manifested by the streaky lines along the fast scan direction in the image. Fig. 5b is an image taken from the same area as that in (a) but after  $\sim 5$  min of continuous scan. As a result, some weakly adsorbed stuff has been swept away from this area and the image becomes clearer. The swept away material is seen to be re-deposited at step edges where some very bright (tall) features have appeared. Fig. 5c is an image taken after an additional  $\sim$ min of scanning. By now, there is hardly any material left on the flat terraces and the number of bright features along the step edges has clearly increased. Fig. 5d

is a zoomed-in view of the area inside the black square in (c). In this image, there is no PtO in view, the small bright spots in Fig. 5d are due to atomic oxygen attached to carbon atoms. The linear feature running diagonally from top left to lower right is a mismatch boundary between two grains of graphite.

In order to evaluate the thermal stability of the oxide particles, the sample was annealed in vacuum first at 473 K, and then at 773 K and 973 K, 30 min at each temperature. Following the annealing at each temperature, the sample was scanned and the corresponding STM images are shown in Fig. 6. Fig. 6a was obtained after annealing to 473 K. This annealing process has stabilised the small particles which appear much more stable under the STM scan. On the terraces, one can see the branched islands. Each island consists of a number of linked small particles. Fig. 6b was obtained after annealing to 773 K. According to a recent study [34], PtO on a Pt(111) surface decomposes at 700 K, but nanoparticles of PtO supported on silica is stable up to 800 K. At the lower half of image in Fig. 6b, there are a few relatively large fractal islands. Each fractal island consists a large number of linked small particles. The existence of fractal islands suggests that the particles in the islands are still metal oxide in nature. Pt metal would form compact islands at this temperature.

Annealing to 973 K has caused more dramatic changes as shown in Fig. 6c. Now the fractal islands have disappeared and only isolated particles and small bright spots are found in STM images. The small bright spots are from oxygen atoms attached to carbon atoms. The isolated particles are of metallic Pt because 973 K is above the decomposition temperature of PtO nanoparticles [34]. When we deposited Pt metal onto HOPG at 723 K, we found no stable structure of Pt on the terraces, Fig. 4. However, stable structure of Pt metal is observed in Fig. 6c. Here the stability of Pt clusters on the terrace is due to the presence of oxygen atoms. Oxygen atoms form chemical bond with surface carbon atoms. At the same time, oxygen atoms can trap Pt atoms. Fig. 6d displays height profiles for PtO and Pt particles at different stages of thermal annealing. Fig. 6e shows the particle height distribution for PtO particles based on images similar to that shown in Fig. 6a. We have performed a simple experiment in which we use the STM tip to physically push the Pt atoms away. Every time we do this, we find an oxygen-induced bright spots at the location where the Pt cluster sat. One of such oxygen-induced features is shown in Fig. 6f.

#### 4. Conclusions

A thermal cracking source has been developed to co-deposit Pt and atomic oxygen onto graphite. The binding of atomic oxygen to surface carbon atoms on HOPG creates strong pinning sites where PtO particles are attached. Thermal annealing experiments show that the PtO particles are stable up to 773 K. Higher temperature causes thermal decomposition of the PtO, which leads to the formation of dispersed metallic Pt particles at the initial pinning sites.

#### Acknowledgement

We thank the Engineering and Physical Sciences Research Council (EPSRC) of the United Kingdom for financial support.

#### References

- [1] C.R. Henry, Surf. Sci. Rep. 31 (1998) 235.
- [2] J. Libuda, H.J. Freund, Surf. Sci. Rep. 57 (2005) 157.
- [3] C.R. Henry, Prog. Surf. Sci. 80 (2005) 92.
- [4] C.T. Campbell, Surf. Sci. Rep. 27 (1997) 1.
- [5] M.A. Brown, Y. Fujimori, F. Ringleb, X. Shao, F. Stavale, N. Nilius, M. Freund, H.J. Sterrerand, J. Am. Chem. Soc. 133 (2011) 10668.
- [6] J. Taing, M.H. Chengand, J.C. Hemminger, ACS Nano 5 (2011) 6325.

- [7] L.K. Ono, B. Yuan, H. Heinrich, B.R. Cuenya, *J. Phys. Chem. C* 114 (2010) 22119.
- [8] S.J. Tauster, S.C. Fung, R.L. Garten, *J. Am. Chem. Soc.* 100 (1979) 170.
- [9] S.J. Tauster, *Acc. Chem. Res.* 20 (1987) 389.
- [10] D.W. Goodman, *Catal. Lett.* 99 (2005) 1.
- [11] M. Bowker, P. Stone, P. Morrall, R. Smith, R. Bennett, N. Perkins, R. Kvon, C. Pang, E. Fourre, M. Hall, *J. Catal.* 234 (2005) 172.
- [12] D.R. Mullins, K.Z. Zhang, *Surf. Sci.* 513 (2002) 163.
- [13] Q. Guo, R.W. Joyner, *Appl. Surf. Sci.* 144–145 (1999) 375.
- [14] E. Ganz, K. Sattler, J. Clarke, *Surf. Sci.* 219 (1989) 33.
- [15] L.J. Lewis, P. Jensen, N. Comb, J.L. Barrat, *Phys. Rev. B* 61 (2000) 16084.
- [16] J.H. Ryu, H.Y. Kim, D.H. Kim, D.H. Seo, H.M. Lee, *J. Phys. Chem. C* 114 (2010) 2022.
- [17] P. Jensen, X. Blasé, P. Ordejon, *Surf. Sci.* 564 (2004) 173.
- [18] Q. Guo, P. Fallon, J. Yin, R.E. Palmer, *Adv. Mater.* 15 (2003) 1084.
- [19] F. Yin, C. Xirouchaki, Q. Guo, R.E. Palmer, *Adv. Mater.* 17 (2005) 121.
- [20] L. Chen, A. Yelon, E. Sacher, *J. Phys. Chem. C* 115 (2011) 7896.
- [21] K. Fauth, M. Hessler, D. Batchelor, G. Schultz, *Surf. Sci.* 529 (2003) 397.
- [22] D.Q. Yang, E. Sacher, *Surf. Sci.* 516 (2002) 43.
- [23] L. Bardotti, P. Jensen, A. Hoareau, M. Treilleux, B. Cabaud, *Phys. Rev. Lett.* 74 (1995) 4694.
- [24] S.J. Carroll, K. Seeger, R.E. Palmer, *Appl. Phys. Lett.* 72 (1998) 305.
- [25] S. Gibilisco, M. Di Vece, S. Palomba, G. Faraci, R.E. Palmer, *J. Chem. Phys.* 125 (2006) 084704.
- [26] H. Hobvel, I. Barke, *Prog. Surf. Sci.* 81 (2006) 53.
- [27] S. Watcharinyanon, C. Virojanadara, L.I. Johansson, *Surf. Sci.* 605 (2011) 1918.
- [28] Z.H. Zhou, F. Gao, D.W. Goodman, *Surf. Sci.* 604 (2010) 1071.
- [29] R. Zan, U. Bangert, Q. Ramasse, K.S. Novoselov, *Small* 7 (2011) 2868.
- [30] A. Guerrero-Ruiz, P. Badenes, I. Rodriguez-Ramos, *Appl. Catal., A* 173 (1998) 313.
- [31] E. Antolini, *J. Mater. Sci.* 38 (2003) 2995.
- [32] Q. Ma, R.A. Rosenberg, *Phys. Rev. B* 60 (1999) 2827.
- [33] S.W. Poon, J.S. Pan, E.S. Tok, *Phys. Chem. Chem. Phys.* 8 (2006) 3326.
- [34] L.K. Ono, J.R. Croy, H. Heinrich, B.R. Cuenya, *J. Phys. Chem. C* 115 (2011) 16856.